

Broadband Terahertz Time-domain Spectroscopy of Quantum Materials in a Dilution Refrigerator

R. J. Vukelich,^{1, a)} T. Norden,^{1, a)} T. G. Hastings,² M. Giri,¹ M. Caldwell,¹ S. Forutan,¹ J. L. Reno,³ and D. J. Hilton¹

¹⁾*Department of Physics, Baylor University, Waco, TX, 76798-7316, USA*

²⁾*Department of Physics, University of Alabama at Birmingham, Birmingham, AL, 35294-1170, USA*

³⁾*Center for Integrated Nanotechnologies, Sandia National Laboratories, Albuquerque, New Mexico 87185, USA*

(*Electronic mail: David_Hilton@baylor.edu)

(Dated: 19 January 2026)

We have constructed a terahertz time domain spectroscopy system using a Bluefors dilution refrigerator with a 7 T split-coil magnet. Using a gallium arsenide single quantum well sample, terahertz waveforms were measured at 145 mK in a magnetic field range from 0 to 6 Tesla to measure cyclotron resonance. Effective mass is found to be $0.073m_e$, which is larger than the commonly accepted bulk value of $0.068m_e$.

I. INTRODUCTION

Quantum materials have electronic and optical properties governed by *nontrivial* quantum mechanical interactions¹. The understanding of the physics of quantum materials is critical for the development of next-generation electronic and optical devices. In addition to the recent developments in quantum computers^{2,3}, quantum sensors and other quantum devices also rely on operation at these temperatures and, therefore on the electronic phase of materials near their ground state⁴⁻⁸.

Modern electronics and optoelectronics are generally dependent on either Group III-V (e.g., GaAs⁹, Al_xGa_{1-x}As⁹) or Group IV (e.g., Si¹⁰, SiGe¹¹, Ge^{12,13}) semiconducting compounds. These conventional semiconductors and metals still require a quantum mechanical description via band structure theory, but their properties can be largely described within the single-particle approximation^{14,15} or with, at most, weakly interacting systems¹⁶ at all but the lowest of temperatures. These are, as a result, generally not classified as quantum materials¹.

The dependence of quantum materials on *non-trivial* interactions and wavefunction interference leads to a wide diversity of emergent behavior. One of the earliest examples of quantum behavior in materials was the observation of the integer (IQHE)¹⁷ and later fractional (FQHE)¹⁸ quantum Hall effect in two-dimensional silicon and gallium arsenide samples. The IQHE and FQHE result from the formation of edge states in quantized Landau levels due to the interference of electron wavefunctions in the edge states, which results in the formation of off-diagonal conductivity plateaus¹⁹. Other classes of quantum materials include both conventional²⁰ and unconventional superconductors²¹, Weyl semimetals²², and other topological materials²³⁻²⁷. An extensive recent review of quantum materials and their applications can be found in ref. 28.

Materials development by serendipity has been a common

pathway for many classical and quantum materials²⁹. *Design* of quantum materials is challenging due to their strong dependence on these complex interactions³⁰. A number of empirical and quantitative rules aid in the development of conventional materials³¹, while the corresponding design rules for quantum materials are less well-developed³²⁻³⁵. The development of novel experimental tools that can elucidate these quantum interactions is critically needed to permit the development of new quantum materials.

Optics-based experiments provide direct spectroscopic information on the relevant energy scales of these interactions over a wider range of excitation energies than are accessible to transport techniques³⁰. Ultrafast experimental techniques can complement these measurements by probing the *dynamics* of coupling between different degrees of freedom in quantum materials³⁶. In this manuscript, we describe the development of a broadband ultrafast terahertz time-domain spectroscopy experiment. Our experiment has a bandwidth of $0.3 \text{ THz} \leq \nu \leq 7.0 \text{ THz}$ that is generated via frequency mixing of near-infrared femtosecond pulses in a plasma^{37,38}. Terahertz pulses were collected in transmission geometry through our samples and detected using THz-ABCD detection methods³⁹ at temperatures $T \geq 145 \text{ mK}$ and in external magnetic fields ($-7 \text{ T} \leq B \leq +7 \text{ T}$). To circumvent the limitations of fiber optics at these frequencies, our system employs free-space operation. The terahertz pulses are generated outside the dilution refrigerator, transmitted through the sample chamber via suitable optical windows, and then detected outside the refrigerator. After outlining our design decisions, we demonstrate the functionality of our instrument by studying cyclotron resonance in a Landau-quantized two-dimensional electron gas sample^{40,42,43}. These measurements represent the first ultrafast terahertz optical study of materials at sub-300 mK⁴², opening a new experimental regime for the characterization and development of quantum materials.

^{a)}Contributed equally to this manuscript.

II. BACKGROUND

A. Transport-based characterization

Low-temperature characterization techniques have been extensively employed to study the complex and often competing interactions between electronic, lattice, spin, and orbital degrees of freedom in materials⁴⁴⁻⁴⁷. In the case of quantum materials, multiple experimental techniques can be needed to unravel the complex competition between these degrees of freedom⁴⁸. The study of materials at temperatures below ≈ 1 K typically requires specialized hardware and sophisticated cooling techniques to provide sufficient cooling power to reach these temperatures⁴⁹⁻⁵¹. Low-temperature measurements of quantum materials have been enabled by the development of the dilution refrigerator⁴⁹⁻⁵³. Dilution refrigerators exploit the phase separation of mixtures of He-3/He-4 below $T = 0.8$ K into a surface He-3 rich phase and the remaining He-3 poor phases⁵⁴. He-3 atoms from the rich phase move into the He-3 poor phase and absorb heat (enthalpy) to do so. This He-3 is extracted from the mixture and recirculated through the system to allow the mixing chamber to reach temperatures below 10 mK.

Characterization of materials at temperatures below 1 K has traditionally been performed using transport-based techniques. This allows for the sample chamber to be isolated from ambient conditions without the need for optical windows and reduces the heat load on the sample^{55,56}. There has been significant development of high-sensitivity techniques to measure electrical properties that can maintain this thermal isolation of the sample space that is necessary to reach these low temperatures. Measurements of specific heat^{55,57,58} and resistivity/conductivity are common and the interpretation of these results has enabled the elucidation of the properties of these materials⁵⁹.

B. Optics-based characterization

Optical spectroscopy of condensed matter systems permits us to measure the absorption, reflection, and transmission of materials across a wide range of photon energies, from the microwave through the x-ray, and over a broad range of time scales, from the femtosecond (10^{-15} ps) to time-integrated measurements over an extended time frame. Each wavelength range is sensitive to different electronic processes in the material that is being studied. In semiconductors and metals, the free carrier response can be studied using microwave⁶⁰ and/or terahertz spectroscopy^{61,62}. In superconducting samples, both of these frequency ranges study the Cooper pairs in the superconducting condensate and can be used to determine the pairing energy and quasiparticle density⁶³. On the other end of the spectrum, the x-ray response results in photoemission of electrons^{64,65} or by the generation of a diffraction pattern^{64,66} that can be used to characterize the crystalline order of materials⁶⁷. The choice of photon energy range under study determines the materials physics under test.

Optical fibers are one method of light delivery into the sample chamber⁶⁸⁻⁷⁰ in the absence of windows. Fiber and other waveguide coupling techniques are often used with these low-temperature spectroscopy experiments to enable delivery of visible or near-infrared light into the sample space and to collect the transmitted or reflected light for analysis⁷¹. At these wavelengths, optical fibers are usually based on fused silica near its dispersion or loss minima⁷². Ultrafast delivery of broadband pulses would be significantly degraded by material dispersion, which will stretch the pulse duration and limit the temporal resolution of the system⁷³. Nonlinear phenomena such as Brillouin scattering^{72,74} can complicate pulse propagation, as well, and lead to power transmission limit or unstable frequency spectra due to supercontinuum generation⁷⁵.

Our instrument design focuses on generation and detection of terahertz light over the spectrum from 0.3 THz $\leq v \leq 7.0$ THz. Metal waveguides are one method for guided terahertz light. This couples the terahertz light to the surface plasmon mode of a stainless steel rod for long term transport⁷⁶. The configuration in ref. 76 has bandwidth that is limited by the source to 0.1 THz to 1.0 THz and has limited coupling efficiency between its linearly polarized source and the radially polarized ($E \sim \hat{r}E_R$) surface plasmon-polariton mode, which limits its utility for spectroscopic applications. Other alternatives based on hollow waveguides⁷⁷ and all-polymer waveguides⁷⁸ suffer from limited bandwidth and mode dispersion that would make them difficult to use with broadband ultrafast terahertz sources.

Ref. 69 recently demonstrated Fourier Transform Infrared (FTIR) spectroscopy measurements in a dilution refrigerator at temperatures as low as 43 mK. FTIR is a highly flexible platform that is capable of operating over a wide range of the electromagnetic spectrum if a set of suitable light sources and beam splitters are available. This method is able to provide important information about a wide range of optical conductivities for materials in equilibrium. Their system employed either a globar or a mercury arc lamp as the incoherent light source from 0.25 THz ($h\nu = 1$ meV) to 250 THz ($h\nu = 1$ eV). This light is then coupled via free-space optical windows into the dilution refrigerator. While FTIR has been previously demonstrated to have broad utility⁴⁸ to characterize quantum materials, approaches based on *coherent* sources in the far infrared and terahertz have been shown to have advantages over incoherent sources for high mobility materials⁷⁹.

THz spectroscopy using a hollow metal waveguide in a dilution refrigerator has been previously reported⁸⁰. Here, the THz was generated using a quantum cascade laser (QCL) inside of a dilution refrigerator with a central frequency of 2.6 THz. They demonstrated an operating temperature of 160 mK at the mixing chamber and an electron temperature at the sample of ~ 430 mK while measuring cyclotron resonance. This technique has recently been modified to be done in free space within the dilution refrigerator and has seen a significant reduction in thermal loading, with an operating temperature of 47 mK⁸¹. Potential limitations with this method include the fixed narrow band output commonly seen in QCL's, which does not easily allow for the broadband experiments that we will demonstrate in this manuscript.

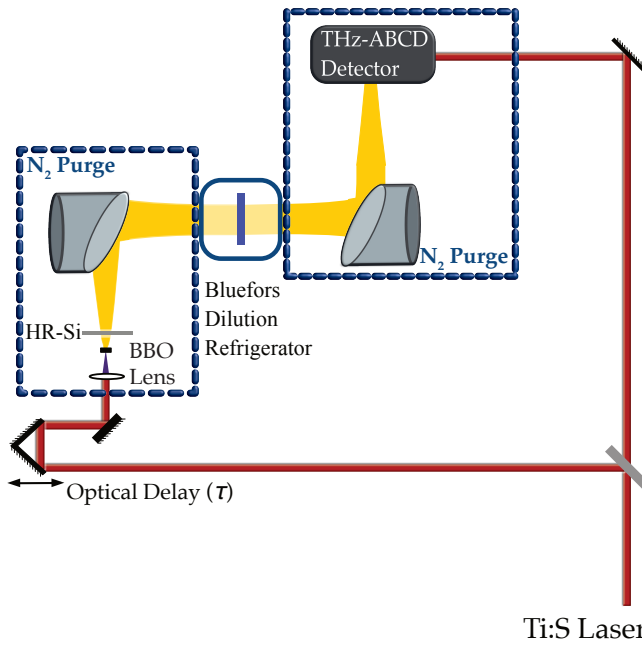


FIG. 1. We generate terahertz pulses by mixing the fundamental [$\lambda_1 = 800$ nm] and second harmonic [$\lambda_2 = 400$ nm, generated using β – BaB_2O_4 (BBO)] of the titanium:sapphire output in a plasma filament in air³⁷. Terahertz emission is separated from the residual visible light using a high-resistivity silicon filter (HR-Si). This is then collected by an off axis parabolic mirror into the Bluefors dilution refrigerator. Optical windows in and out of the sample chamber are TPX (polymethylpentene), which has adequate transmission in both the visible and over our terahertz bandwidth⁸⁹. After the dilution refrigerator windows, the transmitted light is incident on a custom-constructed THz-ABCD detector⁹⁰, which we use to recover the electric field, $\vec{E}(\tau)$, of the transmitted THz pulse.

C. Ultrafast optics-based characterization

Ultrafast optical spectroscopy techniques permit us to study these materials far from equilibrium. We can use these to determine how the system returns to equilibrium and the time-scales on which it does so. Ultrafast sources typically use broadband, subpicosecond pulsed lasers in a pump-probe⁸², transient four-wave mixing⁸³, time-resolved photoluminescence⁸⁴ or other experimental configuration to study the nonlinear susceptibility of materials⁸⁵. These experiments use broadband sources and high peak amplitudes that often exclude the potential of using dispersive waveguides that will necessarily compromise the time-resolution of the experiment^{86–88}.

III. INSTRUMENT DESIGN

A diagram of our experimental setup is shown in Figure 1. We use an ultrafast amplified titanium:sapphire laser system to generate linearly-polarized broadband ($0.3 \text{ THz} \leq v \leq 7.0 \text{ THz}$) terahertz pulses by mixing the fundamental

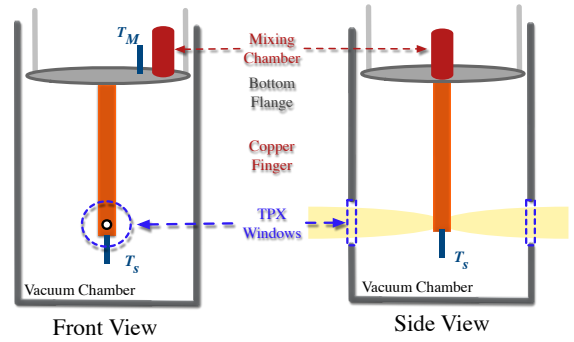


FIG. 2. Inside the dilution refrigerator, the lowest flange has the He-3/He-4 mixing chamber along with a co-located temperature sensor (T_S). We have custom constructed a copper cold finger that is in thermal contact via an indium foil seal with the lowest flange. The cold finger has a 1 cm transmission aperture that is aligned with the TPX optical windows. A second temperature sensor (RuOx Sensor, Model number: A01892, T_S) is attached to the copper finger at the sample position and will be the reported sample temperature in this manuscript. Samples are mounted on the transmission aperture using GE 7031 varnish, which ensures good thermal contact between the cold finger and sample⁹¹. (Not shown) There are three internal radiation shields with a pair of windows each. This results in eight TPX windows on the full beam path.

($\lambda_1 = 800$ nm) and second harmonic ($\lambda_2 = 400$ nm) in a plasma^{37,38}. We generate the plasma at the focus on the titanium:sapphire laser beam in nitrogen and generate the second harmonic of the beam using a β – BaB_2O_4 single crystal. To block the residual 800 nm and 400 nm light, we use a 1 cm thick high resistivity silicon window as a visible light filter to block all but the generated terahertz light from transmission into our dilution refrigerator. We use a pair of off-axis parabolic mirrors to guide the terahertz beam from the plasma filament into the sample chamber and to collect the transmitted beam and bring it to our THz-ABCD detector⁹⁰.

A simplified diagram of the dilution refrigerator chamber is included as Figure 2. In the Bluefors system, the bottom flange has the He-3/He-4 mixing chamber and a temperature sensor (T_S). This is typically $T_S \approx 10 \text{ mK}$ at the base temperature of our experiment. We mount our sample on a custom-constructed copper finger that is in good thermal contact via an indium foil seal with the bottom flange. This custom copper finger has a $d = 1 \text{ cm}$ hole on which we mount our samples to measure the transmitted terahertz light. This design positions the sample in the terahertz beam path through the TPX windows while maintaining thermal contact with the mixing chamber. A second temperature sensor (T_S) is located on the bottom of our copper finger close to the sample; this is the sensor recording used for all temperature readings in the experiments described in this manuscript.

A. Design Criteria

Specific design criteria for our apparatus include:

I. Broadband THz generation and detection: We use

a broadband ultrafast terahertz spectrometer similar to the one described in ref. 92. This generates terahertz by frequency mixing of the fundamental and second harmonic of a titanium:sapphire laser in air⁹³. We detect these using the THz-ABCD detector geometry described in ref. 94. This system will have a broad bandwidth to achieve subpicosecond time-resolution or, equivalently, the bandwidth will span from 0.3 THz ($h\nu = 1.2$ meV) to the edge of the terahertz transmission window in our TPX windows, which is beyond 7 THz ($h\nu = 29.0$ meV)⁹⁵.

II. Low-temperature operation in the quantum limit:

This experiment will allow for the study of materials using ultrafast terahertz sources at temperatures below $T_S \leq 200$ mK ($k_B T_S \leq 17.2$ μ eV). Normalized energy scales, $x = \frac{h\nu}{k_B T_S}$ in this geometry can be as large as $x \approx 1,700$, demonstrating the ability of our setup to probe samples in the quantum limit where thermal fluctuations are minimized. To do so, we use external generation and detection methods to minimize internal heat load in the sample chamber³². We also restrict the solid angle into the sample chamber to minimize the effects of stray light into the sample position. When we replace the optical windows with metallic plugs, the sample temperature is below $T_S \leq 6$ mK. Thus, the base temperature in our experiment is limited by the transmission of the optical windows and our success in isolating the sample chamber from the ambient. Proper thermal management of ambient radiation into the sample chamber is an area of future system optimization to reduce our base sample temperature below the current $T_S = 145$ mK to extend this deeper into the quantum limit (i.e., larger x).

III. External magnetic field:

Our system includes an integrated 7 T split-coil magnet to enable us to study materials at low temperature and external magnetic field in both the Faraday ($\vec{B} \parallel \vec{k}$) and Voigt geometries ($\vec{B} \perp \vec{k}$), where \vec{k} is the propagation vector of the terahertz field. This is below the critical magnetic fields for several superconducting systems of interest (e.g., $B_{c2} \approx 15$ to 20 T in many cuprates⁶³ and even higher in iron-based superconductors^{32,96,97}), which will require specialized facilities to study^{98,99}.

IV. Coherent control:

The use of ultrafast optical sources in our design instead of blackbody-type sources of terahertz radiation is, in part, motivated by their ability to control the electronic wave function¹⁰⁰ and potentially access hidden order in materials¹⁰¹. In this context, hidden order emerges when the external stimulus significantly contributes to the equation of state of the system and results in the emergence of a novel electronic, structural, or magnetic phase not otherwise present in the absence of this stimulus. Recently developed *tabletop* ultrashort terahertz emission sources¹⁰²⁻¹⁰⁴ are capable of nonperturbatively exciting the sample with picosecond pulses with electric fields on the same order of magni-

tude or larger than the internal mean fields^{105,106}. While this manuscript will focus on single pulse spectroscopy, straightforward extensions to our configuration will permit coherent control experiments in the future^{107,108}.

B. System Components

Our system consists of four main components: a laser source, a terahertz generator, a terahertz detector, and a free-space optics-compatible dilution refrigerator. The use of free-space optical techniques simplifies the experiment design as it allows for both the generation and detection *outside* of the cryostat.

A. Titanium:sapphire laser amplifier: The system uses a femtosecond laser regenerative amplifier [Spectra Physics Solstice Ace, $\sigma = 35$ fs, $\mathcal{U} = 7$ mJ per pulse, $\lambda_0 = 800$ nm ($h\nu_0 = 1.55$ eV)] to generate terahertz pulses. A 90% reflective beamsplitter is used for the terahertz generation path and gate path, respectively. To generate terahertz pulses for both Faraday and Voigt geometries, this generation pulse is split by a 50:50 beamsplitter, resulting in 3.15 mJ pulses that are used for both geometries. In this paper, we focus on the Faraday geometry generation path used to observe cyclotron resonances in a gallium arsenide quantum well sample.

B. Terahertz time domain spectroscopy via plasma generation: Terahertz pulses are generated using the method of gas-ionization. The fundamental pulse, ν_0 , of the Ti:S is focused through a $\beta - \text{Ba}_2\text{BO}_4$ (β -barium borate) Type-I cut crystal in a nitrogen purged box, resulting in a collinear second harmonic pulse at $2\nu_0$. A photocurrent is induced in the ionized nitrogen as the electrons move away from the ions when there is a phase difference between the ω and 2ω photons at the focus^{104,109}. The result of this induced photocurrent is the generation of ultrafast terahertz radiation with ~ 1 μ W of average power, along with a white light continuum, that is reflected off an off-axis parabolic. A high resistivity silicon filter is used to separate the broadband terahertz frequencies from the high frequency components of the white light generation and the residual titanium:sapphire beam.

C. Air-based coherent detection: An air-based coherent detector is used to detect the terahertz pulses¹¹⁰. After transmission through the dilution refrigerator, the terahertz pulse is focused by an off-axis parabolic between two copper electrodes. These copper electrodes are spaced apart 1.5 mm and connected to an Advanced Energy Ultravolt 2 kV bipolar high voltage amplifier, resulting in a modulated bias field within the capacitive gap. The biased field is modulated using a custom circuit creating a bipolar signal modulated at half the frequency of the titanium:sapphire amplifier's repetition rate. This allows the bipolar biased field to simulate a quasi-second-order nonlinear process, allowing

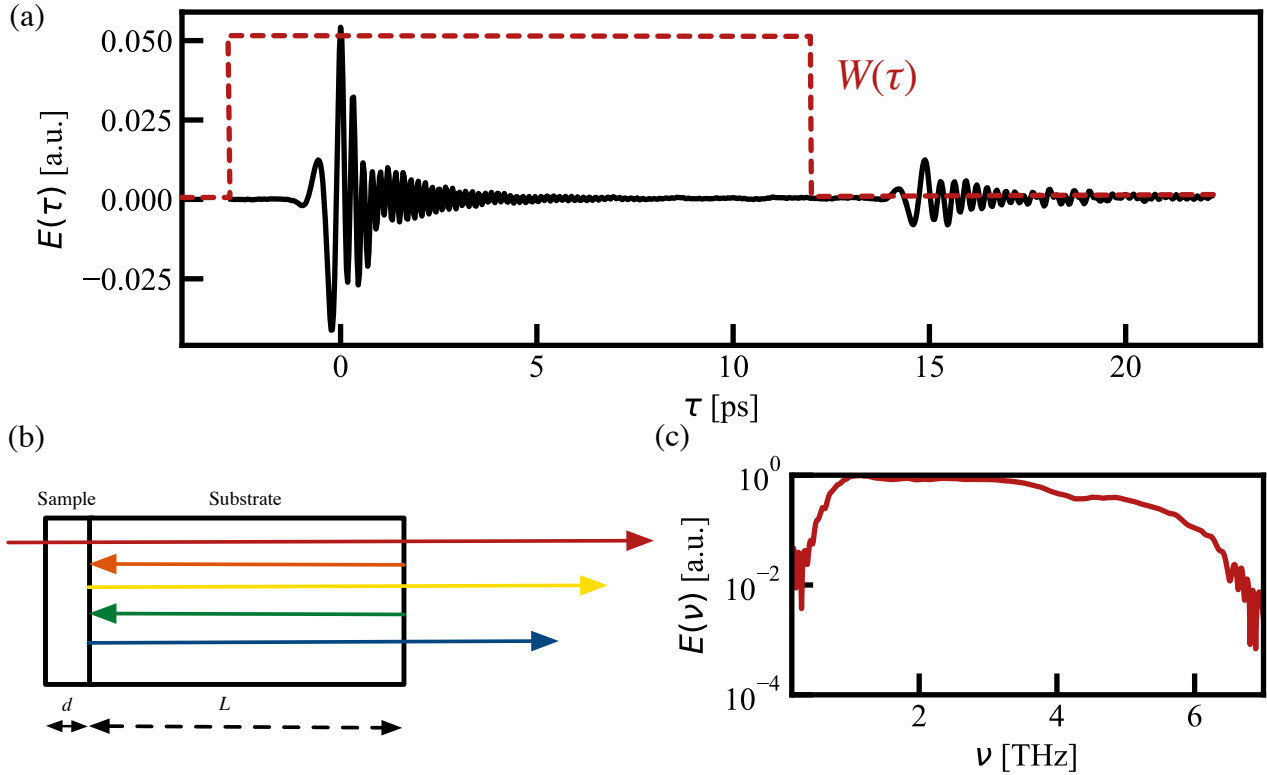


FIG. 3. (a) A representative THz Waveform, $E(\tau)$, and the numerical window, $W(\tau)$ with a width of $\tau_W = 15$ ps applied to our data to remove secondary pulse reflections. (b) This is a simplified diagram of our sample (Sample ID: VA0605), consisting of the two dimensional layer (d) and a thick GaAs substrate (L). The windowed $E_W(\tau)$ is the single pass waveform through the structure and removes the multiple reflections/etalon from the calculated spectrum. (b) A schematic diagram of the sample, showing the origin of the multiple reflections in the time-domain or, equivalently, of the Fabry-Perot interference fringes in the frequency domain. (c) The FFT of numerically windowed spectrum from the first pass through the sample.

for the coherent detection of the terahertz pulse by using a Newport Femtowatt Detector to detect the filtered 400 nanometer generation created by the terahertz pulse, gate pulse, and biased field mixing. This signal is sent to a lock-in which is locked to half the titanium:sapphire amplifier's repetition rate.

D. Dilution refrigerator: A Bluefors LD-400 dilution refrigerator is used to cool samples down to the mK range. The dilution refrigerator is a cryogen-free system that has two perpendicular optical axes through an external shield (room temperature), radiation shield (50 K), 7 T cryogen-free horizontal field split-coil magnet (American Magnetics, Inc.) that can be replaced by a second radiation shield (4 K), and still tail (800 mK). A He-4 compressor in a closed system is used to initially cool down to liquid helium temperatures, where a He-3/He-4 mixture can be introduced to be precooled. After the mixture is precooled, it can be condensed to a state where He-4 is pulled to the bottom of the dilution chamber by gravity and the He-3 is forced through the condensed He-4. The resulting osmotic pressure cools the dilution chamber down to mK temperature, which is connected to the mixing chamber flange. Available optical axes allow us to conduct measurements in ei-

ther Faraday or Voigt geometries when a sample is in the dilution refrigerator. Each optical axis consists of four optical windows before and after the sample, for a total of eight optical apertures (not shown in Figure 2). For this experiment, TPX polymethylpentene windows were used in the Faraday axis optical apertures.

E. Sample mount: A custom copper cold finger with optical aperture has been connected to the mixing chamber flange and extends down so the sample mount's aperture is aligned with the optical axis of the external shield windows. GE Varnish is used to mount samples to the cold finger and copper tape is used to ensure there are no gaps between the sample and cold finger aperture through which terahertz radiation is transmitted. To provide an accurate temperature measure at the sample position, a second temperature sensor is connected to the bottom of the cold finger in proximity to the sample. The cold finger can be rotated 90 degrees to allow for measurements in Faraday ($\vec{k} \perp \vec{B}$) or Voigt ($\vec{k} \parallel \vec{B}$) geometries.

F. Cryostat windows: Our broadband generation is limited by the transmission of the windows used in this cryostat. A wide range of different materials can be

used for this frequency range, including diamond, sapphire, silicon, and quartz as well as multiple plastics including polyethylene, polymethylpentene (TPX), and Polytetrafluoroethylene (Teflon)^{111,112}. We have chosen 1 mm thick TPX windows for our system, which is motivated by its high transmission in both the terahertz as well as in the visible/near infrared¹¹³.

IV. RESULTS AND DISCUSSION

We use our apparatus to study cyclotron resonance in a high mobility two-dimensional electron gas (2DEG). Recent work has emphasized new 2D materials based on monolayer semiconductors^{114–118} as well as monolayer transition metal dichalcogenides. This has also extended into multilayer systems with controlled twist angles to directly engineer the electronic and optical properties of these materials¹¹⁹. While these provide significant methods for designing and controlling the electronic properties of the 2DEG, growth of high mobility samples that are predicted to have the longest coherence lifetimes are enabled by high-purity III-V molecular beam epitaxy¹²⁰. High mobility two-dimensional systems are known to have narrow band and magnetically tunable resonances that will permit us to examine the resolution limits of our system and plan for future upgrades and motivate the development of new analysis methods for future use.

Our sample is a gallium arsenide quantum well (Sample ID: VA0605) doped to an electron concentration of $n_s \approx 4 \times 10^{11} \text{ cm}^{-2}$ that is grown via molecular beam epitaxy¹²¹. In the presence of an external magnetic field, the states split into a discrete spectrum of equally spaced Landau levels, $E_n = n\hbar\omega_{CR}$, separated by the cyclotron energy. These Landau levels are broadened by sample-dependent disorder that results from lattice impurities and defects in the material⁴³. These levels are also broadened by the collective emission of this ensemble of dipoles as superradiant emission¹²², which makes the decay time result from both phenomena, depending on the temperature range⁴³. These Landau levels result in a strong circular dichroism near the cyclotron energy that results from a transition between the highest filled and lowest unfilled Landau levels with dephasing time determined by the sample disorder⁴³.

The sample temperature was measured to be $T_S = 141 \text{ mK}$ without the incident THz beam incident on the sample. With the THz incident, the base temperature at the sample location rose to $T_S = 145 \text{ mK}$, indicating there is minimal heating from the laser source. Terahertz time-domain spectroscopy waveforms were measured at $T_S = 145 \text{ mK}$ in a gallium arsenide 18 nanometer single quantum well (VA0605) for magnetic fields from 0 to 6 T in 0.5 T steps. A waveform measured with no magnetic field is shown in Figure 3(a). The waveform shows the main terahertz pulse and the first satellite pulse, due to internal reflections within the gallium arsenide substrate. An example of the internal reflections and the satellite pulses produced is shown in Figure 3(b). The separation between the main pulse and satellite pulse is similar to that found by Ref. 92 of approximately $\tau_W = 15 \text{ ps}$ and is determined by the

substrate thickness on which this sample is grown.

We numerically window the acquired THz pulse $E_W(\tau) = W(\tau) \times E(\tau)$ with a window length of $\tau_W = 15 \text{ ps}$ to remove the etalon from our TPX windows. We calculate the complex spectrum, $\tilde{E}(v) = E(v) \exp(i\varphi)$ of our terahertz pulses using the fast-Fourier transform of the windowed terahertz waveform measured without a magnetic field. The magnitude of the spectrum, $E(v)$, is shown in Figure 3(c); the phase, φ , is not shown. The broadband spectrum of the waveform is cutoff at 7 THz due to the eight TPX windows plus sample that the waveform needs to transmit through the dilution refrigerator. The low frequency cutoff is limited by diffraction¹²⁴.

To demonstrate the system with the 7 T magnet, cyclotron resonance in our sample is measured from 0.5 T to 6 T; we do not reach the full 7 T in this experiment as the cyclotron resonance frequency in gallium arsenide is above the usable bandwidth of our pulse at those fields. The resulting cyclotron resonance waveforms are shown in Figure 4(a). The isolated cyclotron resonance is found by subtracting the zero magnetic field waveform, $E(\tau, 0)$, from the waveforms at the B -field strengths labeled on the right side in Figure 4(a), $E(\tau, B)$, to generate $\Delta E(\tau, B) = E(\tau, B) - E(\tau, 0)$. To obtain the values of the cyclotron resonances, we compute the fast-Fourier transforms of $\Delta E(\tau, B)$ measured from 1.5 to 6 T. These are shown in Figure 4(b) as a function of the frequency for each value of B .

To determine the effective mass of the gallium arsenide single quantum well sample, the cyclotron frequency, v_c , of each curve in Figure 4(b) is fitted using a Gaussian curve plus a linear component, where the center of the Gaussian fit is taken to be the cyclotron frequency. An example fitting is shown in Figure 4(c), where the value of the cyclotron frequency is $v_c = 1.53 \text{ THz}$ from these fittings at $B = 4.0 \text{ T}$. The cyclotron frequency all values of the magnetic field are shown in Figure 4(d). Using these cyclotron frequencies, a linear fit was used to determine the effective mass of the sample which was found to be $0.073 m_e$, where m_e is the electron mass. This effective mass is larger than was reported in a similar experiment in Ref. 43. This may be related to the stronger confinement effects in this sample and will be the subject of a future investigation by our group¹²⁵.

V. CONCLUSIONS AND FUTURE DIRECTIONS

Broadband terahertz time domain spectroscopy was performed using a dilution refrigerator with a 7 T magnet to measure the cyclotron resonance of gallium arsenide single quantum wells below $T_S = 300 \text{ mK}$. The zero magnetic field waveform and its fast-Fourier transform verifies our capability to transmit a broadband terahertz waveform through the dilution refrigerator and sample, and perform a measurement on the opposite side of the dilution refrigeration than the generation. Cyclotron resonance measurements on a gallium arsenide single quantum well were performed to verify the use of the 7 T magnet with the broadband terahertz at $T_S = 145 \text{ mK}$.

Our ability to perform broadband terahertz spectroscopy in a dilution refrigerator, with or without the 7 T magnet, will

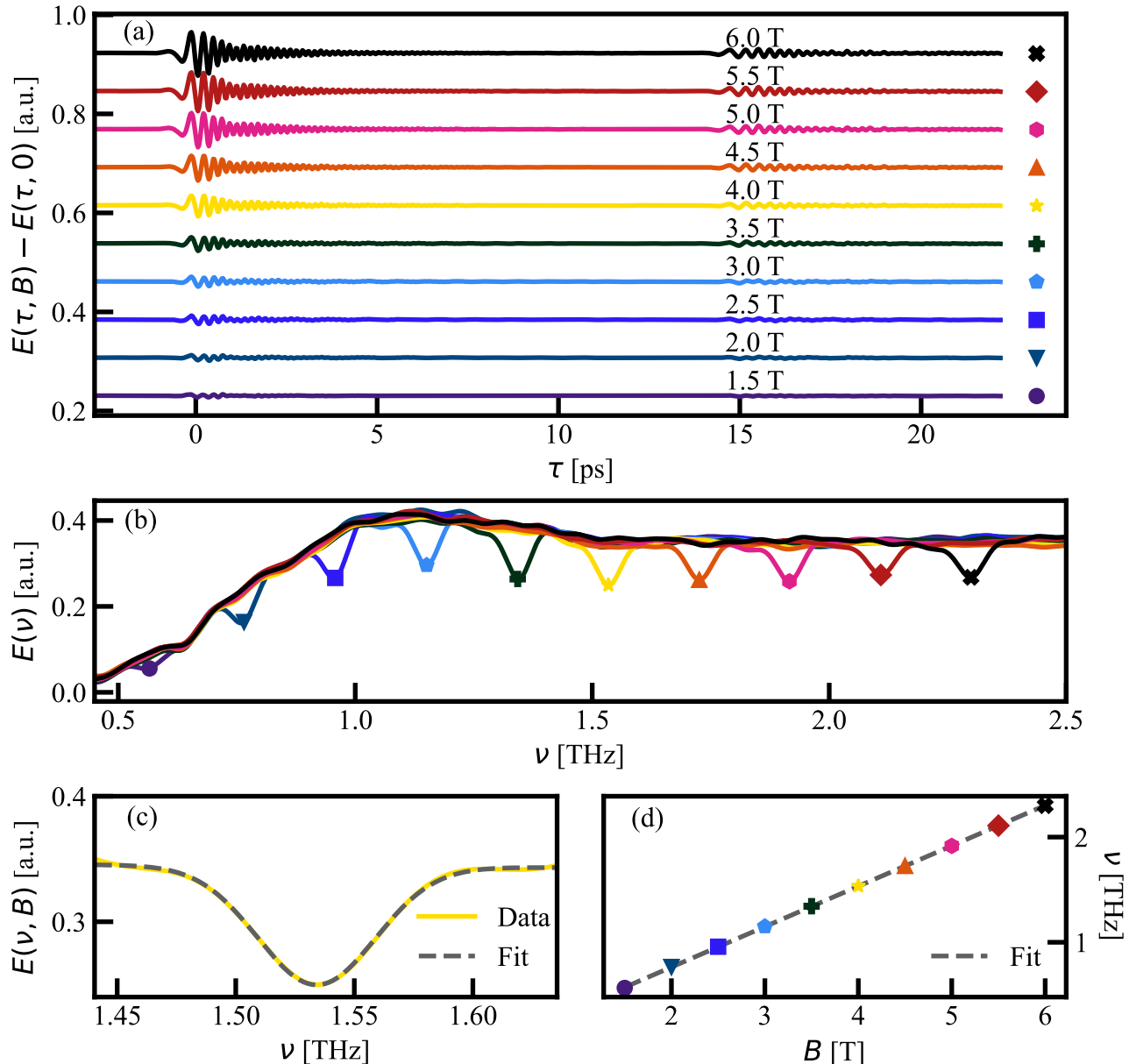


FIG. 4. (a) The change to the transmitted terahertz waveforms at B when compared to the zero field transmitted THz waveform at 145 mK for 1.5 T to 6.0 T. For fields below 1.5 T and above 6.0 T, the cyclotron resonance in GaAs is at a frequency outside of our experiments spectral bandwidth ($0.3 \text{ THz} \leq \nu \leq 7.0 \text{ THz}$). (b) Frequency spectra of the measured waveforms calculated by taking the fast Fourier transform of the waveform data in (a). (c) A representative fitting of the spectrum line shape to a homogeneously broadened Lorentzian line shape¹²³. (d) The central frequency, $\nu_c(B)$ is shown on as a function of B . We determine the effective mass from the slope of this fitting, as discussed within the text and in Ref 40. The line width, $\Delta\nu$ is instrument-response limited in our apparatus by the TPX window thickness and will be the focus of future development efforts.

allow us to probe nonequilibrium dynamics of quantum materials in a temperature regime previously inaccessible to broadband terahertz systems. By generating the terahertz external to the dilution refrigerator, the portion of the titanium:sapphire laser not used for terahertz generation or detection could be utilized in other ways, such as a second terahertz generation path to perform two dimensional terahertz spectroscopy or as a pump beam using either the fundamental or a harmonic. These additional uses would strengthen the ability of this sys-

tem to understand the exotic quantum ground states seen at mK temperatures.

CONFLICT OF INTERESTS

The authors have no conflicts to disclose.

AUTHOR CONTRIBUTIONS

R. J. Vukelich: Investigation (equal), Formal Analysis (co-lead), Visualization (lead), Software (supporting), Writing/Original Draft Preparation (co-lead); **T. Norden:** Investigation (equal), Formal Analysis (co-lead), Software (lead); **T. G. Hastings:** Investigation (supporting), Writing/Review & Editing (supporting); **M. Giri:** Investigation (supporting), Writing/Review & Editing (supporting); **M. Caldwell:** Investigation (supporting); **S. Fourtan:** Writing/Review & Editing (supporting); **D. J. Hilton:** Conceptualization (lead), Funding Acquisition, Project Administration (lead), Supervision (lead), Visualization (supporting), Formal Analysis (supporting), Writing/Original Draft Preparation (co-lead), Writing/Review & Editing (co-lead)

ACKNOWLEDGMENTS

THz Detector Development was supported by the National Science Foundation under grant DMR-1919944. This work was performed, in part, at the Center for Integrated Nanotechnologies, an Office of Science User Facility operated for the U.S. Department of Energy (DOE) Office of Science by Los Alamos National Laboratory (Contract 89233218CNA000001) and Sandia National Laboratories (Contract DE-NA-0003525).

DATA AVAILABILITY STATEMENT

The data that support the findings of this study are openly available in the *figshare* repository at <http://doi.org/10.6084/m9.figshare.31075618>, reference number [10.6084/m9.figshare.31075618].

BIBLIOGRAPHY

- 1R. Cava, N. d. Leon, and W. Xie, *Chemical Reviews* **121**, 2777 (2021).
- 2G. Q. A. Collaboration, *Nature* , 1 (2024).
- 3M. A. Quantum, M. Aghaei, A. A. Ramirez, Z. Alam, R. Ali, M. Andrzejczuk, A. Antipov, M. Astafev, A. Barzegar, B. Bauer, J. Becker, U. K. Bhaskar, A. Bocharov, S. Boddapati, D. Bohn, J. Bommer, L. Bourdet, A. Bousquet, S. Boutin, L. Casparis, B. J. Chapman, S. Chattoor, A. W. Christensen, C. Chua, P. Codd, W. Cole, P. Cooper, F. Corsetti, A. Cui, P. Dalpasso, J. P. Dehollaing, G. d. Lange, M. d. Moor, A. Ekefjärd, T. E. Dandachi, J. C. E. Saldaña, S. Fallahi, L. Galletti, G. Gardner, D. Govender, F. Griggio, R. Grigoryan, S. Grijalva, S. Gronin, J. Gukelberger, M. Hamdast, F. Hamze, E. B. Hansen, S. Heedt, Z. Heidarnia, J. H. Zamorano, S. Ho, L. Holgaard, J. Hornibrook, J. Indrapiromkul, H. Ingerslev, L. Ivancevic, T. Jensen, J. Jhoja, J. Jones, K. V. Kalashnikov, R. Kallaher, R. Kalra, F. Karimi, T. Karzig, E. King, M. E. Kloster, C. Knapp, D. Kocon, J. V. Koski, P. Kostamo, M. Kumar, T. Laeven, T. Larsen, J. Lee, K. Lee, G. Leum, K. Li, T. Lindemann, M. Looij, J. Love, M. Lucas, R. Lutchyn, M. H. Madsen, N. Madulid, A. Malmros, M. Manfra, D. Mantri, S. B. Markussen, E. Martinez, M. Mattila, R. McNeil, A. B. Mei, R. V. Mishmash, G. Mohandas, C. Mollgaard, T. Morgan, G. Moussa, C. Nayak, J. H. Nielsen, J. M. Nielsen, W. H. P. Nielsen, B. Nijholt, M. Nystrom, E. O'Farrell, T. Ohki, K. Otani,

- 4B. P. Wütz, S. Pauka, K. Petersson, L. Petit, D. Pikulin, G. Prawiroatmodjo, F. Preiss, E. P. Morejon, M. Rajpalke, C. Ranta, K. Rasmussen, D. Razmadze, O. Reentila, D. J. Reilly, Y. Ren, K. Reneris, R. Rouse, I. Sadovskyy, L. Sainiemi, I. Sanlorenzo, E. Schmidgall, C. Sfiligoj, M. B. Shah, K. Simoes, S. Singh, S. Sinha, T. Soerensen, P. Sohr, T. Stankevici, L. Stek, E. Stuppard, H. Suominen, J. Suter, S. Teicher, N. Thiyagarajah, R. Tholapi, M. Thomas, E. Toomey, J. Tracy, M. Turley, S. Upadhyay, I. Urban, K. V. Hoogdalem, D. J. V. Woerkom, D. V. Viazmitinov, D. Vogel, J. Watson, A. Webster, J. Weston, G. W. Winkler, D. Xu, C. K. Yang, E. Yucelen, R. Zeisel, G. Zheng, and J. Zilke, *Nature* **638**, 651 (2025).

- 5B. J. M. Hausmann, I. Bulu, V. Venkataraman, P. Deotare, and M. Lončar, *Nature Photonics* **8**, 369 (2014).

- 6C. L. Degen, F. Reinhard, and P. Cappellaro, *Reviews of Modern Physics* **89**, 035002 (2017), 1611.02427.

- 7N. Aslam, H. Zhou, E. K. Urbach, M. J. Turner, R. L. Walsworth, M. D. Lukin, and H. Park, *Nature Reviews Physics* **5**, 157 (2023).

- 8T. Esat, D. Borodin, J. Oh, A. J. Heinrich, F. S. Tautz, Y. Bae, and R. Temirov, *Nature Nanotechnology* **19**, 1466 (2024).

- 9S. Adachi, *Journal of Applied Physics* **58**, R1 (1985).

- 10J. Luttinger and W. Kohn, *Physical Review* **97**, 869 (1955).

- 11M. L. Lee, E. A. Fitzgerald, M. T. Bulsara, M. T. Currie, and A. Lochtefeld, *Journal of Applied Physics* **97**, 011101 (2005).

- 12J. Luttinger and W. Kohn, *Physical Review* **97**, 869–883 (1955).

- 13J. M. Luttinger, *Physical Review* **102**, 1030–1041 (1956).

- 14W. Brandt and J. Reinheimer, *Physical Review B* **2**, 3104 (1970).

- 15S. Adachi, *Physical Review B* **41**, 1003–1013 (1990).

- 16W. Hanke and L. J. Sham, *Physical Review Letters* **43**, 387 (1979).

- 17K. von Klitzing, G. Dorda, and M. Pepper, *Physical Review Letters* **45**, 494 (1980).

- 18D. C. Tsui, H. Stormer, and A. C. Gossard, *Physical Review Letters* **48**, 1559 (1982).

- 19R. Laughlin, *Physical Review B* **23**, 5632 (1981).

- 20J. Bardeen, *Physical Review Letters* **1**, 399 (1958).

- 21J. Bednorz and K. A. Müller, *Z. Phys. B: Condens. Matt.* **64**, 189–193 (1986).

- 22B. Yan and C. Felser, *Annual Review of Condensed Matter Physics* **8**, 1 (2016), 1611.04182.

- 23A. B. Sushkov, G. S. Jenkins, D. C. Schmadel, and N. P. Butch, *Physical Review B* **82** (2010), 10.1103/physrevb.82.125110.

- 24G. S. Jenkins, A. B. Sushkov, D. C. Schmadel, N. P. Butch, P. Syers, J. Paglione, and H. D. Drew, *Physical Review B* **82**, 125120 (2010).

- 25M. Neupane, S.-Y. Xu, L. A. Wray, A. Petersen, R. Shankar, N. Alidoust, C. Liu, A. Fedorov, H. Ji, J. M. Allred, Y. S. Hor, T.-R. Chang, H.-T. Jeng, H. Lin, A. Bansil, R. J. Cava, and M. Z. Hasan, *Physical Review B* **85**, 235406 (2012).

- 26R. V. Aguilar, A. V. Stier, W. Liu, L. S. Bilbro, D. K. George, N. Bansal, L. Wu, J. Cerne, A. G. Markelz, S. Oh, and N. P. Armitage, *Physical Review Letters* **108**, 087403 (2012), 1105.0237.

- 27L. Luo, X. Yang, X. Liu, Z. Liu, C. Vaswani, D. Cheng, M. Mootz, X. Zhao, Y. Yao, C.-Z. Wang, K.-M. Ho, I. E. Perakis, M. Dobrowolska, J. K. Furdyna, and J. Wang, *Nature Communications* **10**, 1 (2019).

- 28A. Zong, B. R. Nebgen, S.-C. Lin, J. A. Spies, and M. Zuerch, *Nature Reviews Materials* **8**, 224 (2023).

- 29S. V. Kalinin, B. G. Sumpter, and R. K. Archibald, *Nature Materials* **14**, 973 (2015).

- 30D. N. Basov, R. D. Averitt, and D. Hsieh, *Nature Materials* **16**, 1077–1088 (2017).

- 31J. Xie, Y. Zhou, M. Faizan, Z. Li, T. Li, Y. Fu, X. Wang, and L. Zhang, *Nature Computational Science* **4**, 322 (2024).

- 32B. Keimer and J. E. Moore, *Nature Physics* **13**, 1045 (2017).

- 33C. Ahn, A. Cavalleri, A. Georges, S. Ismail-Beigi, A. J. Millis, and J.-M. Triscone, *Nature Materials* **20**, 1462 (2021).

- 34F. Giustino, J. H. Lee, F. Trier, M. Bibes, S. M. Winter, R. Valent, Y.-W. Son, L. Taillefer, C. Heil, A. I. Figueroa, B. Plaais, Q. Wu, O. V. Yazyev, E. P. A. M. Bakkers, J. Nygrd, P. Forn-Daz, S. D. Franceschi, J. W. McIver, L. E. F. F. Torres, T. Low, A. Kumar, R. Galceran, S. O. Valenzuela, M. V. Costache, A. Manchon, E.-A. Kim, G. R. Schleider, A. Fazzio, and

S. Roche, *Journal of Physics: Materials* **3**, 042006 (2020), 2102.02644.

³⁵N. Marzari, A. Ferretti, and C. Wolverton, *Nature Materials* **20**, 736 (2021).

³⁶D. Fausti, R. I. Tobe, N. Dean, S. Kaiser, A. Dienst, M. C. Hoffmann, S. Pyon, T. Takayama, H. Takagi, and A. Cavalleri, *Science* **331**, 189 (2011).

³⁷K.-Y. Kim, A. J. Taylor, J. H. Glownia, and G. Rodriguez, *Nature Photonics* **2**, 605 (2008).

³⁸N. Karpowicz, X. Lu, and X. C. Zhang, *Laser Physics* **19**, 1535–1539 (2009).

³⁹X. Lu, N. Karpowicz, and X. C. Zhang, *Journal of the Optical Society of America B: Optical Physics* **26**, A66 (2009).

⁴⁰X. Wang, D. J. Hilton, L. Ren, D. M. Mittleman, J. Kono, and J. L. Reno, *Optics Letters* **32**, 1845 (2007).

⁴¹X. Wang, D. J. Hilton, D. M. Mittleman, J. Kono, and J. L. Reno, “Time-domain terahertz magneto-spectroscopy of an ultrahigh-mobility two-dimensional electron gas,” (2008).

⁴²J. A. Curtis, T. Tokumoto, A. T. Hatke, J. G. Cherian, J. L. Reno, S. A. McGill, D. Karaikaj, and D. J. Hilton, *Physical Review B* **93**, 155437 (2016).

⁴³B. Barman, A. G. Linn, A. L. O’Beirne, J. Holleman, C. Garcia, V. Mapara, J. L. Reno, S. A. McGill, V. Turkowski, D. Karaikaj, and D. J. Hilton, *Journal of Physics: Condensed Matter* **35**, 305302 (2023).

⁴⁴L. J. v. d. Pauw, *Phillips Research Reports* **13**, 1 (1958).

⁴⁵G. T. Meaden, *Contemporary Physics* **12**, 313 (1971).

⁴⁶I. Miccoli, F. Edler, H. Pfür, and C. Tegenkamp, *Journal of Physics: Condensed Matter* **27**, 223201 (2015).

⁴⁷D. N. Basov, R. D. Averitt, D. v. d. Marel, M. Dressel, and K. Haule, *Reviews of Modern Physics* **83**, 471 (2011).

⁴⁸D. N. Basov, R. D. Averitt, and D. Hsieh, *Nature Materials* **16**, 1077 (2017).

⁴⁹H. London, G. R. Clarke, and E. Mendoza, *Physical Review* **128**, 1992 (1962).

⁵⁰H. Hall, P. Ford, and K. Thompson, *Cryogenics* **6**, 80 (1966).

⁵¹J. C. Wheatley, O. E. Vilches, and W. R. Abel, *Physics Physique Fizika* **4**, 1 (1968).

⁵²T. Hata, T. Matsumoto, K. Obara, H. Yano, O. Ishikawa, A. Handa, S. Togitani, and T. Nishitani, *Journal of Low Temperature Physics* **175**, 471 (2014).

⁵³H. Cao, *Journal of Low Temperature Physics* **204**, 175 (2021).

⁵⁴L. Goldstein, *Physical Review* **95**, 869 (1953).

⁵⁵G. R. Stewart, *Review of Scientific Instruments* **54**, 1 (1983).

⁵⁶F. Pobell, *Matter and Methods at Low Temperatures* (Springer-Verlag Berlin, Heidelberg, 2007).

⁵⁷R. Bachmann, F. J. DiSalvo, T. H. Geballe, R. L. Greene, R. E. Howard, C. N. King, H. C. Kirsch, K. N. Lee, R. E. Schwall, H. U. Thomas, and R. B. Zubeck, *Review of Scientific Instruments* **43**, 205 (1972).

⁵⁸H. Wilhelm, T. Lugo, J. Albrecht, R. Lortz, and T. Lümann, *Review of Scientific Instruments* **75**, 2705 (2004).

⁵⁹J. Pellegrino *et al.*, *Review of Scientific Instruments* **87**, 044702 (2016).

⁶⁰M. E. Brodwin and R. J. Vernon, *Physical Review* **140**, A1390 (1965).

⁶¹C. Schmuttenmaer, *Chemical Reviews* **104**, 1759 (2004).

⁶²J. Lloyd-Hughes and T.-I. Jeon, *Journal of Infrared, Millimeter, and Terahertz Waves* **33**, 871 (2012).

⁶³D. N. Basov and T. Timusk, *Reviews of Modern Physics* **77**, 721 (2005).

⁶⁴D. A. Nagaoka, L. Hostert, R. V. Gelamo, C. M. Maroneze, D. M. d. Andrade, A. R. Cadore, and C. J. d. Matos, *Applied Surface Science* **695**, 162864 (2025).

⁶⁵P. van der Heide, *X-ray Photoelectron Spectroscopy: An introduction to Principles and Practices*, 1st ed. (Wiley, Hoboken, NJ, 2011).

⁶⁶Y. Waseda, E. Matsubara, and K. Shinoda, *X-Ray Diffraction Crystallography*, 1st ed. (Springer, Heidelberg, 2011).

⁶⁷A. P. Hammersley, *Journal of Applied Crystallography* **49**, 646 (2016).

⁶⁸S. Crooker, *Review of Scientific Instruments* **73**, 3258 (2002).

⁶⁹M. Onyszczak, A. J. Uzan-Narolansky, Y. Tang, P. Wang, Y. Jia, G. Yu, T. Song, R. Singha, J. F. Khouri, L. M. Schoop, and S. Wu, *Review of Scientific Instruments* **94**, 103903 (2023), 2308.00610.

⁷⁰T. Hamamoto, A. Blunia, H. Takahashi, and Y. Kubo, *Review of Scientific Instruments* **96**, 085201 (2025), 2501.18938.

⁷¹K. Ciesiolkiewicz, J. Kopaczek, and R. Kudrawiec, *ACS Applied Optical Materials* **3**, 1995 (2025).

⁷²G. Agrawal, *Nonlinear Fiber Optics, Third Edition (Optics and Photonics)*, 3rd ed., Academic Press (Academic Press, 2001).

⁷³W. Göbel, A. Nimmerjahn, and F. Helmchen, *Optics Letters* **29**, 1285 (2004).

⁷⁴J.-i. Kosugi and Y. Takagi, *Japanese Journal of Applied Physics* **38**, 3069 (1999).

⁷⁵A. Gaeta, *Physical Review Letters* **84**, 3582 (2000).

⁷⁶K. Wang and D. M. Mittleman, *Nature* **432**, 376 (2004).

⁷⁷N. Arunkumar, R. H. Giles, T. Goyette, J. Kumar, and W. E. Nixon, *Terahertz Physics, Devices, and Systems IV: Advanced Applications in Industry and Defense*, 76710S (2010).

⁷⁸D. Wang, *International Symposium on Photoelectronic Detection and Imaging 2011: Terahertz Wave Technologies and Applications*, 819512 (2011).

⁷⁹M. Chou, D. Tsui, and G. Weimann, *Physical Review B* **37**, 848 (1988).

⁸⁰M. Vaughan, W. Michailow, M. Salih, L. Li, H. Beere, D. A. Ritchie, E. H. Linfield, A. G. Davies, and J. E. Cunningham, *Review of Scientific Instruments* **93**, 113906 (2022).

⁸¹M. T. Vaughan, W. Michailow, R. Xia, L. Li, M. Salih, H. E. Beere, D. A. Ritchie, E. H. Linfield, A. G. Davies, J. R. Freeman, and J. E. Cunningham, *Review of Scientific Instruments* **96**, 063901 (2025).

⁸²R. Prasankumar and A. Taylor, eds., *Optical Techniques for Solid-State Materials Characterization*, 1st ed. (CRC Press, New York, 2011).

⁸³A. D. Bristow, D. Karaikaj, X. Dai, T. Zhang, C. Carlsson, K. R. Hagen, R. Jimenez, and S. Cundiff, *Review of Scientific Instruments* **80**, 073108 (2009).

⁸⁴M. Achermann, “Optical techniques for solid-state materials characterization,” (CRC Press, 2016) p. 466–489.

⁸⁵R. Boyd and S. Mukamel, *Physical Review A* **29**, 1973 (1984).

⁸⁶D. G. Ouzounov, *Science* **301**, 1702 (2003).

⁸⁷A. Chong, W. H. Renninger, and F. W. Wise, *Optics Letters* **32**, 2408 (2007).

⁸⁸J. Phoenix, L. Gaudreau, M. Korkusinski, P. Zawadzki, A. Bogan, S. Stednichenko, R. L. Williams, and A. S. Sachrajda, *Review of Scientific Instruments* **91**, 083107 (2020).

⁸⁹J. Bichon, A. Pillet, A. Sklia, D. Petitprez, R. Peretti, and S. Eliet, *2022 47th International Conference on Infrared, Millimeter and Terahertz Waves (IRMMW-THz)* **00**, 1 (2022).

⁹⁰I.-C. Ho, X. C. Zhang, and X. Guo, *Optics Express* **18**, 2872 (2010).

⁹¹R. Stephens, *Cryogenics* **15**, 420 (1975).

⁹²J. A. Curtis, A. D. Burch, B. Barman, A. G. Linn, L. M. McClintock, A. L. O’Beirne, M. J. Stiles, J. L. Reno, S. A. McGill, D. Karaikaj, and D. J. Hilton, *Review of Scientific Instruments* **89** (2018), 10.1063/1.5023384.

⁹³N. Karpowicz, X. Lu, and X. C. Zhang, *Journal of Modern Optics* **56**, 1137 (2009).

⁹⁴X. Lu, N. Karpowicz, and X. C. Zhang, *Journal of the Optical Society of America B: Optical Physics* **26**, A66 (2009).

⁹⁵A. Podzorov and G. Gallot, *Applied Optics* **47**, 3254 (2008).

⁹⁶J. Paglione and R. L. Greene, *Nature Physics* **6**, 645 (2010).

⁹⁷R. M. Fernandes, A. I. Coldea, H. Ding, I. R. Fisher, P. J. Hirschfeld, and G. Kotliar, *Nature* **601**, 35 (2021).

⁹⁸J. Toth, M. D. Bird, S. Bole, and J. W. O'Reilly, *Applied Superconductivity, IEEE Transactions on* **22**, 4301604 (2012).

⁹⁹J. A. Curtis, T. Tokumoto, N. K. Nolan, L. M. McClintock, J. G. Cherian, S. A. McGill, and D. J. Hilton, *Optics Letters* **39**, 5772 (2014).

¹⁰⁰T. Arikawa, X. Wang, D. J. Hilton, J. L. Reno, W. Pan, and J. Kono, *Physical Review B* **84**, 241307 (2011).

¹⁰¹X. Wei, C. Tian, H. Cui, Y. Zhai, Y. Li, S. Liu, Y. Song, Y. Feng, M. Huang, Z. Wang, Y. Liu, Q. Xiong, Y. Yao, X. C. Xie, and J.-H. Chen, *Nature Communications* **15**, 5038 (2024).

¹⁰²J. Hebling, *Optical and Quantum Electronics* **28**, 1759 (1996).

¹⁰³J. Hebling, M. C. Hoffmann, H. Y. Hwang, K.-L. Yeh, and K. A. Nelson, *Physical Review B* **81**, 035201 (2010).

¹⁰⁴K. Y. Kim, A. J. Taylor, J. H. Glownia, and G. Rodriguez, *Nature Photonics* **2**, 605 (2008).

¹⁰⁵H. Aoki, N. Tsuji, M. Eckstein, M. Kollar, T. Oka, and P. Werner, *Reviews of Modern Physics* **86**, 779 (2014).

¹⁰⁶C.-J. Yang, J. Li, M. Fiebig, and S. Pal, *Nature Reviews Materials* **8**, 518 (2023).

¹⁰⁷T. Arikawa, X. Wang, D. J. Hilton, J. L. Reno, W. Pan, and J. Kono, *Physical Review B* **84**, 241307 (2011).

¹⁰⁸M. Woerner, W. Kuehn, P. Bowlan, K. Reimann, and T. Elsaesser, *New Journal of Physics* **15**, 025039 (2013).

¹⁰⁹K.-Y. Kim, J. H. Glownia, A. J. Taylor, and G. Rodriguez, *Optics Express* **15**, 4577 (2007).

¹¹⁰X. Lu and X.-C. Zhang, *Frontiers of Optoelectronics* **7**, 121 (2014).

¹¹¹C. Schmuttenmaer, *Chemical reviews* **104**, 1759 (2004).

¹¹²J. Lloyd-Hughes and T.-I. Jeon, *Journal of Infrared, Millimeter, and Terahertz Waves* **33**, 871 (2012).

¹¹³J. A. Curtis, T. Tokumoto, N. K. Nolan, L. M. McClintock, J. G. Cherian, S. A. McGill, and D. J. Hilton, *Optics Letters* **39**, 5772 (2014).

¹¹⁴K. I. Bolotin, F. Ghahari, M. D. Shulman, H. L. Stormer, and P. Kim, *Nature* **462**, 196 (2009).

¹¹⁵P. Vogt, P. D. Padova, C. Quaresima, J. Avila, E. Frantzeskakis, M. Asensio, A. Resta, B. Ealet, and G. L. Lay, *Physical Review Letters* **108**, 155501 (2012).

¹¹⁶L. Tao, E. Cinquanta, D. Chiappe, C. Grazianetti, M. Fanciulli, M. Dubey, A. Molle, and D. Akinwande, *Nature Nanotechnology* **10**, 227 (2015).

¹¹⁷M. E. Dávila, L. Xian, S. Cahangirov, A. Rubio, and G. L. Lay, *New Journal of Physics* **16**, 095002 (2014).

¹¹⁸F.-f. Zhu, W.-j. Chen, Y. Xu, C.-L. Gao, D.-d. Guan, C.-h. Liu, D. Qian, S.-C. Zhang, and J.-F. Jia, *Nature Materials* **14**, 1020 (2015).

¹¹⁹S. Carr, D. Massatt, S. Fang, P. Cazeaux, M. Luskin, and E. Kaxiras, *Physical Review B* **95**, 075420 (2017), 1611.00649.

¹²⁰M. J. Manfra, *Annual Review of Condensed Matter Physics* **5**, 347 (2014).

¹²¹H. Störmer, R. Dingle, A. Gossard, W. Wiegmann, and M. Sturge, *Solid State Communications* **29**, 705 (1979).

¹²²Y. D. Jho, X. Wang, J. Kono, D. H. Reitze, X. Wei, A. A. Belyanin, V. V. Kocharovskiy, V. V. Kocharovskiy, and G. S. Solomon, *Physical Review Letters* **96**, 237401 (2006).

¹²³D. J. Hilton, *Optics Express* **20**, 29717 (2012).

¹²⁴D. You and P. H. Bucksbaum, *Journal of the Optical Society of America B* **14**, 1651 (1997).

¹²⁵H. Sigg, P. Wyder, and J. A. A. J. Perenboom, *Physical Review B* **31**, 5253 (1985).